TOPICAL REVIEW

Resisting oxygen/moisture permeation in quantum dots converted optoelectronic devices

IOP Publishing Journal of Physics D: Applied Physics
J. Phys. D: Appl. Phys. **57** (2024) 483001 (16pp) https://doi.org/10.1088/1361-6463/ad759d

Topical Review

Resisting oxygen/moisture permeation in quantum dots converted optoelectronic devices

Xuan Yang[1], **Bin Xie**[2,*] **and Xiaobing Luo**[1,*]

[1] School of Energy and Power Engineering, Huazhong University of Science and Technology, Wuhan 430074, People's Republic of China
[2] School of Mechanical Science and Engineering, Huazhong University of Science and Technology, Wuhan 430074, People's Republic of China

E-mail: binxie@hust.edu.cn and luoxb@hust.edu.cn

Received 14 May 2024, revised 30 July 2024
Accepted for publication 30 August 2024
Published 9 September 2024

Abstract

Quantum dots (QDs) are promising semiconducting luminous nanocrystals with superior optoelectronic characteristics. Unfortunately, these nanocrystals are fragile when exposed to humid environment. Oxygen and moisture molecules could erode QDs' structure and degrade their luminous ability, which severely hinders the wide application of QDs in optoelectronic devices. Therefore, it is significantly important to resist oxygen/moisture permeation in the packaging of these QDs converted devices. In this review, we briefly introduce the oxygen/moisture-induced degradation mechanism of QDs and then the permeation theories. Subsequently, we review some strategies for resisting oxygen/moisture permeation from a packaging perspective, and analyze them with the permeation theories. Finally, we outline some future directions for developing efficient oxygen/moisture resistance solutions of QDs converted optoelectronic devices.

Keywords: quantum dots, oxygen/moisture resistance, permeation, packaging

1. Introduction

Quantum dots (QDs) have attracted numerous attention over the past decades as a kind of promising luminous nanocrystals [1–4]. The 2023 Nobel Prize in Chemistry was awarded to three scientists for the discovery and synthesis of this unique material. QDs' remarkable characteristics like high quantum efficiencies and size-tunable narrow emission spectra contribute to a wide application in photovaltics fields such as solar cells [5–7], lasers [8, 9], lighting [10–12], and displays [13–15]. However, QDs still suffer from poor stability while exposed to humid environment. Plenty of researches have proved that oxygen and moisture molecules can damage their strcutures, thus causing ligands detaching, core–shell structure failing and size shrinking which produces trap states (TS) inside QDs. Subsequently, the TSs enhance non-radiative process within QDs during light conversion and decrease the luminous efficiency of QDs [16–22]. As a result, reliability and performance of QDs and QDs-converted optoelectronic devices are seriously threatened, which hinders their further applications.

In recent years, the characteristics, optical performances, and applications of QDs have been extensively discussed by peer researchers. They revealed the mechanism of QDs' degradation and the correlations between structural degradation and performance degradation. Discussions on improvement of QDs' performance and stability were carried out

* Authors to whom any correspondence should be addressed.

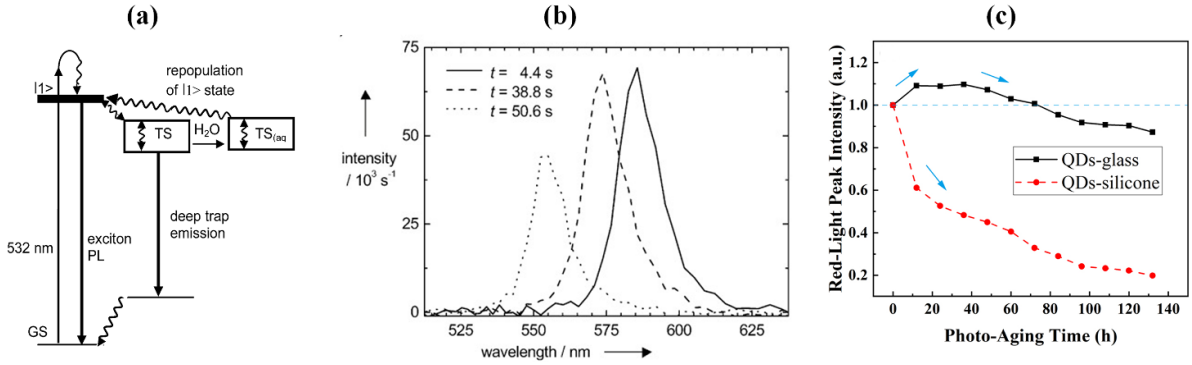

Figure 1. (a) Schematic illustration of the postulated decay route of an exciton generated in CdSe/ZnS quantum dots and the formation of a trap state (TS) and water stabilized trap state ($TS_{(aq)}$). Reprinted with permission from [26]. Copyright (2010) American Chemical Society. (b) Emission spectra of CdSe/ZnS QDs in ambient air at different illumination times. [28] John Wiley & Sons. [© 2002 WILEY-VCH Verlag GmbH & Co. KGaA, Weinheim]. (c) Intensity of QDs in silica glass and silicone under illumination at different times. Reproduced from [32]. © IOP Publishing Ltd. All rights reserved.

from the aspects of materials, synthesis routes and structure design (including design of materials and structure of shell and ligand) [15–19]. Besides the above mentioned strategies on QDs itself, packaging, as a necessary step in the application of QDs, is of great importance to protect QDs from the degradation caused by oxygen and moisture. In QDs-converted optoelectronic devices, QDs are usually dispersed in polymer matrix such as silicone, which serves as a barrier where oxygen and moisture must pass through before contacting with QDs. In general, polymers are formed by crosslinked macromolecules chains where oxygen and moisture molecules are absorbed, dissolved and diffusing. The behavior of oxygen/moisture molecules permeation and QDs degradation are closely correlated. Therefore, studying the perameation behavior of oxygen/moisture in polymer is considerably meaningful and it can pave a way for enhancing oxygen/mositure-resistant ability of QDs' packaging.

In this review, we first briefly introduce the oxygen/moisture-induced degradation mechanism of QDs and their permeation behavior in polymer matrix. Then we reivew the recent advances in packaging-inside oxygen/moisture-resistant strategies for QDs and discuss them with permeation thoeries. Finally, we present a perspective for this field.

2. Basic theory

2.1. Mechanism of oxygen/moisture-induced QDs degradation

Interactions are taken place in humid environment between QDs and oxygen/moisture molecules. Studies indicated that enhancenment and degradation of photoluminesence (PL) intensity exist simultaneously after QDs absorb oxygen and moisture molecules physically or chemically [19, 21, 23–28]. The moisture-induced PL enhancement is always under light illumination, which is also known as photoactivation. This phenomenon is attributed to the passivation of the QDs' surface TSs by aborbed water molecules [19, 23–26]. Figure 1(a) illustrates the mechanism. In this TS mainfold, it can be seen that water molecules could stabilize the TS forming a solvated $TS_{(aq)}$ [26], which is the TS passivation mentioned above. The $TS_{(aq)}$ repopulates electrons from the TS to the conduction band of QDs and enhances band-edge radiative recombination, resulting in a PL enhancement [19, 24, 25]. The photoactivation process can be accelerated by involving oxygen molecules. Take CdSe/CdS QDs as an example, there exists following chemical reaction [23, 29, 30]:

$$CdS + 2H_2O + O_2 \rightarrow Cd^{2+} + SO_4{}^{2-} + 4H^+$$

$$CdSe + H_2O + O_2 \rightarrow Cd^{2+} + SeO_3{}^{2-} + 2H^+.$$

The subsequently formed CdOH or $Cd(OH)_2$ eliminates the TSs of QDs, thus enhancing their PL intensity [23]. Meanwhile, oxygen can cause surface oxidation to QDs forming CdO, SeO_2 and $CdSeO_x$. This process is also known as photooxidation, which passivate the TSs as well as the water molecules [19, 23, 26, 31].

Nevertheless, degradation on optical performances of QDs like reduction of PL intensity, blue-shift of PL spectra and broadening of full width at half maximum (FWHM) (shown in figure 1(b)), is induced when continuously exposed to oxygen and moisture [19, 21, 23, 26–28]. The photo-excited QDs were furtherly oxidized by oxygen and moisture molecules, leading to a gradual erosion of the core and shell and a shrink on their size, which is also called photo-corrosion. The mechanism is that the oxidative dissolution of the formed surface oxidation like CdO, SeO_2 and $CdSeO_x$ occurs and SeO_3^{2-} and Cd^{2+} ions are desorbed from the QDs' surface [23]. As a consequence of that, plenty of TSs are created, and the accompanying enhancement of non-radiative process severely damages optical performance of QDs. Figure 1(c) shows the evolution of PL intensity of QDs in QDs-glass during illumination, it increases at first (photoactivation by passivated TSs), then decreases as the time evolve (degradation by forming TSs) [32].

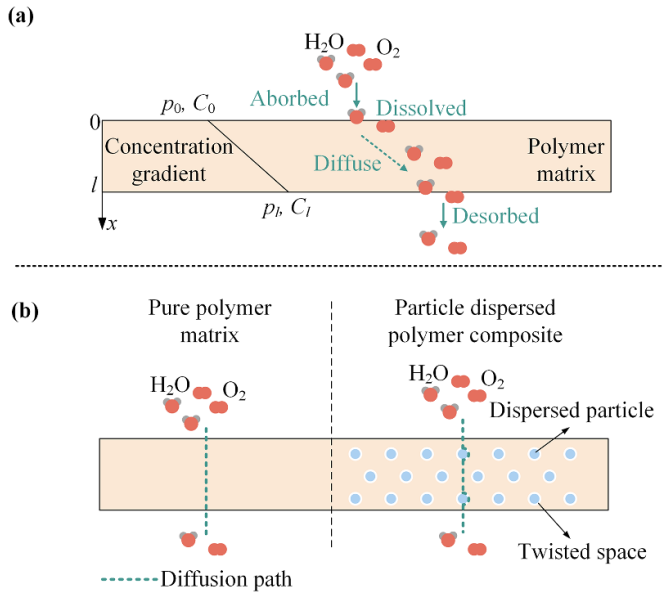

Figure 2. (a) Schematic of the moisture/oxygen molecules permeation process in polymer matrix. (b) Comparison of the diffusion process between pure polymer matrix and particle dispersed polymer composite.

2.2. Permeation thoery of the mositure in packaging

2.2.1. Permeation in polymer matrix. In QDs converted light-emitting devices, QDs are always packaged with polymers such as silicone and epoxy resin for the superior opitcal transparency which is permated by oxygen/moisture molecules in humid environment. Figure 2(a) illustrates the process of permeation described by solution-diffusion model. The permeation of oxygen and moisture molecules in the polymer matrix is driven by the pressure and concentration differnces. The molecules are first aborbed to the top surface of polymer matrix, and then dissolved into polymer phase. Subsequently, they diffuse down the concentration gradient to the bottom surface. Finally, the molecules are desorbed from the matrix [33]. The concentration of oxygen/moisture in the interfaces between air and polymer matrix can be determined as:

$$C = S \times p \tag{1}$$

where C is the concentration of oxygen/moisture (g m^{-3}), S is the solubility of oxygen/moisture in polymer matrix (g m^{-3} Pa^{-1}) and p is the external gas pressure (Pa). The diffusion process follows Fick's law, which gives the rate of diffusion under concentration differences:

$$F = D\frac{\partial C}{\partial x} \tag{2}$$

$$\frac{\partial C}{\partial t} = D\frac{\partial^2 C}{\partial x^2} \tag{3}$$

where F is the mass transfer rate per unit area (g m^{-2} s^{-1}), and D is the diffusion coefficient (m^2 s^{-1}). Equations (2) and (3) are usually referred to as Fick's first and second laws of diffusion, respectively. When it comes to practical systems, the gas surface concentration may not be known but only the gas pressure on the two sides, as shown in figure 2(a). The mass transfer rate can be written as [34]:

$$F = \frac{P(p_0 - p_l)}{l} \tag{4}$$

and

$$P = D \times S \tag{5}$$

where p_0 and p_l are the gas pressure of the top and bottom surface, respectively, l is the thickness of the polymer (m), P is permeation coefficient (g m^{-1} Pa^{-1} s^{-1}). Additionally, in laminates where the layers l_1, l_2, l_3 …l_i are normal to the direction flow, there is [34]:

$$\frac{l_1}{P_1} + \frac{l_2}{P_2} + \ldots \frac{l_i}{P_i} = \frac{l_{\text{total}}}{P_{\text{total}}}. \tag{6}$$

2.2.2. Permeation in inhomogeneous polymer. Embedding QDs into polymer matrix creates an inhomogeneous composite with continuous polymer and dispersed QDs. In some cases, other particles, such as phosphor in white light-emitting diodes, are simultaneously embedded in the polymer along with QDs to produce white light, which enlarged the volume fraction of the dispersed phases. As the volume fraction increases, the effect of the dispersed phases on the permeation characteristics of matrix has to be considered [34–40]. The effective diffusion coefficient of the inhomogeneous composites with spherical dispersed phase can be written as Maxwell's formula [34]:

$$\frac{D_e - D_c}{D_e + 2D_c} = \nu_d \frac{D_d - D_c}{D_d + 2D_c} \tag{7}$$

where D_e, D_c and D_d are the diffusion coefficient of a hypothetical homogenous medium consist of dispersed particles and continuous matrix, continuous matrix, and dispersed particles, respectively. ν_d is the volume fraction of the dispersed particles. In most cases of packaging, the dispersed particles are impermeable with a $D_d = 0$. Equation (7) can be simplified as [41]:

$$D_e = D_c \frac{1 - \nu_d}{1 + \frac{\nu_d}{2}}. \tag{8}$$

The above equation indicates that adding impermeable particles into a polymer matrix could weaken the diffusion. Figure 2(b) shows the diffusion process in an inhomogeneous composite. By creating a twisted space, the dispersion of particles decreases the diffusion with increasing path lengths [36, 39].

Besides, there are some modified models which furtherly consider the interactions of polymer-particles and particle-particles, distribution of particles, and surface effects [38, 42–45]. Higuchi model describes the dielectric properties of two-phase mixtures as follow [43]:

$$P_e = P_c \left[1 + \frac{3\nu_d \lambda}{1 - \nu_d \lambda - K_H (1 - \nu_d)\lambda}\right] \tag{9}$$

and

$$\lambda = \frac{P_d - P_c}{P_d + 2P_c} \tag{10}$$

where P_e, P_c and P_d are the permeation coefficient of a hypothetical homogenous medium consist of dispersed particles and continuous matrix, continuous matrix, and dispersed particles, respectively. λ is a reduced permeability factor featuring permeability difference between the two phases. K_H is an empirical constant affected by sedimentation, aggregation and surface effects of fillers. However, further studies on the permeability of nanoscale particle in polymer have shown that these models were inconsistent with the experimental data in some cases [36–38, 41, 46]. The reason is that they ignore the existing interfaces between polymer matrix and particles [38, 47–49]. Mahajan and Koros proposed to serve the interface as an individual phase independent of polymer and particles. Therefore, a brand new permeation predicting model with three-phase system was developed [50, 51]. Figure 3 gives the concept of this system. In this model, firstly, particles and interfaces are considered as pseudo dispersed phases whose effective permeation coefficient (P_{ps}) is derived from Maxwell formula. Then the effective permeation coefficient of the three-phase system (P_e) is obtained by using Maxwell formula to calculate the system consisting of polymer and the pseudo dispersed phase. Based on this model, Zarabadipoor *et al* proposed to include interfacial morphology and interface thickness, which is written as [38]:

$$P_{ps} = P_I \left[\frac{P_{dB} + 2P_I - 2\nu_s (P_I - P_{dB})}{P_{dB} + 2P_I + \nu_s (P_I - P_{dB})} \right] \tag{11}$$

$$P_{dB} = \gamma \times P_d \tag{12}$$

$$P_I = \beta \times P_c \tag{13}$$

$$P_e = P_c \left[\frac{P_{ps} + 2P_c - 2(\nu_d + \nu_I)(P_c - P_{ps})}{P_{ps} + 2P_c + (\nu_d + \nu_I)(P_c - P_{ps})} \right] \tag{14}$$

where P_{dB} and P_I are the permeation coefficient of affected particles, and interfaces, respectively. γ is the permeability reduction factor of the particle affected by the interface. β is the permeability correction factor of the interphase. ν_s is particle volume fraction in pseudo dispersed phase. ν_I is interface volume fraction in three-phase system.

2.2.3. Temperature-dependent permeation. QDs generate heat during the photoluminescent process in optoelectronic devices, resulting in a high temperature (exceeding 130 °C) of the polymer composite [52]. On one hand, the rising temperature intensifies thermal motion of molecules which is beneficial to the diffusion. On the other hand, since the process of gas dissolution is always exothermic, it is suppressed by the rising temperature. *P, D* and *S* are temperature-dependent described by van't Hoff-Arrhenius model as [53, 54]:

$$P = P_0 \times \exp\left(-\frac{E_p}{RT}\right) \tag{15}$$

$$D = D_0 \times \exp\left(-\frac{E_d}{RT}\right) \tag{16}$$

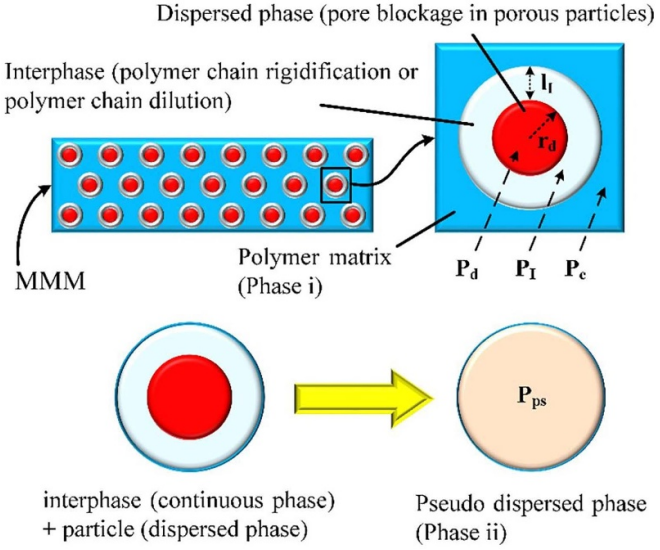

Figure 3. Concept of mixed matrix membranes (MMMS) as three-phase system and the pseudo dispersed phase. Reprinted from [38], Copyright (2021), with permission from Elsevier.

$$S = S_0 \times \exp\left(-\frac{\Delta H_s}{RT}\right) \tag{17}$$

where E_p and E_d are the activation energies of permeability and diffusivity (J mol^{-1}), respectively. ΔH_s is the heat of sorption (J mol^{-1}). P_0, D_0 and S_0 are the corresponding pre-exponential factors. R is the gas content (8.314 J mol^{-1} K^{-1}) and T is the temperature (K). E_d is usually positive while ΔH_s is usually negative, indicating that the rising temperature strengthened diffusion and weakened dissolution [53–59].

3. Packaging-inside oxygen/moisture-resistant strategies for QDs converted optoelectronic devices

In this section, we mainly review the oxygen/moisture-resistant strategies for QDs in weakening the permeation for the aspects of QDs coating, matrixes and packaging structures.

3.1. Micro–nano buffer layer outside QDs

Coating buffer layers ouside QDs has been proved to be an effective strategy which provides protection for QDs in applications under nearly all circumstances. Figure 4 illustrates the schematic that the buffer layers protect QDs from oxygen and moisture molecules. Oxygen and moisture molecules permeate polymer matrix of length l_1 with P_c (green dashed line), and then permeat buffer layer of length l_2 with P_b (bule dashen line), where $P_b < P_c$. The two processes serve as a permeation in a hypothetic phase of length l with P_{cb} (black dashed line), which can be calculated by equation (6):

$$P_{cb} = P_c \frac{l}{l_1 + k_P l_2} \tag{18}$$

where $k_p = P_c/P_b$, which is always smaller than unit.

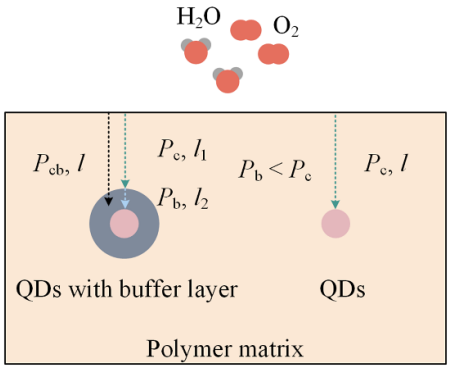

Figure 4. Schematic of permeation of QDs coated with buffer layer.

Silica is the most widely used coating material for its excellent optical transparency and chemical stability [60]. In the past decades, plenty of methods to coat QDs with silica shell have been proposed, which can be devided into two main categories: sol–gel reaction [61–66] and microemulsion reaction [67–75]. The sol–gel reaction is fabricating silica by using siloxane precursors which forms nucleation sites on the QDs' surface under control conditions through hydrolytic polycondensation [76]. Kobayashi *et al* [61] fabricated silica-coated QDs using teraethyl orthosilicate (TEOS) as precursor, NaOH aqueous solution as catalyst to hydrolyze TEOS and ethanol as solvent to form a homogeneous reaction phase. However, in this reaction, NaOH aqueous solution and ethanol are harmful to QDs, leading to a degradation on QDs' photoluminescent properties. Sun *et al* [63] proposed a novel method with a more compatible system for QDs. Figure 5(a) illustrates the fabrication process. With water-free solvent of octadecene, and (3-aminopropyl)triethoxysilane (APTES) that self-silanize without catalyst were adopted to coat QDs. Besides, APTES was also chosen to cap the surface of QDs as ligands thus guaranteeing a well coating of silica. As a result, as seen in figures 5(b) and (c), photoluminescent properties of QDs changed slightly before and after coating silica, and the photoluminescent quantum yield (PLQY) of QD/silica powders was remarkably stable over time, of which red QD/silica powders only showed 5% dorp over three months.

Microemulsion reaction is a water-in-oil process which can control the number of QDs in one bead through changing the concentation of components [67]. Figure 6 illustrates the fabrication process. The reaction system consists of oil phase such as toluene and hexane, surfactants, siloxane precursors, QDs with hydrophobic ligands, small amout of water and catalyst. The hydrophilic ends of surfactants form water phase as micro reactors in oil phase. QDs with hydrophobic ligands are first dispersed in oil phase where their hydrophobic ligands are changed by siloxane precursors. After that, ligand-changed QDs moved into waster-phase micro reactors and coated with silica shell by the hydrolysis of siloxane precursors [67, 68].

Goryacheva *et al* [70] investigated the influence of the silanization conditions on opticla properties of silica-coated QDs using microemulsion reaction. Since surfactants build the water-phase micro reactor in oil sovlent, they determine the size and number of the water phase and influence

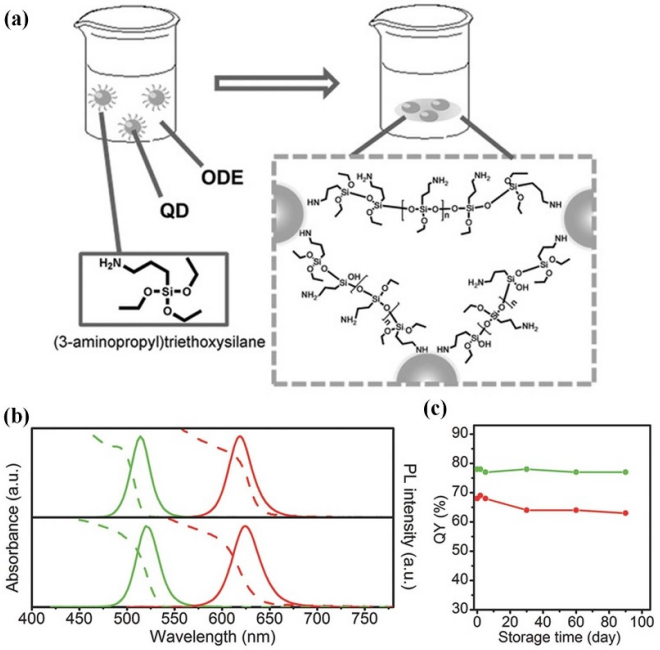

Figure 5. (a) Fabrication process of silica-coated QDs. The absorption (dashed lines) and PL (solid lines) spectra of (b) freshly made green and red QDs in solution (c) green and red QD/silica composites. [63] John Wiley & Sons. [© 2016 WILEY-VCH Verlag GmbH & Co. KGaA, Weinheim].

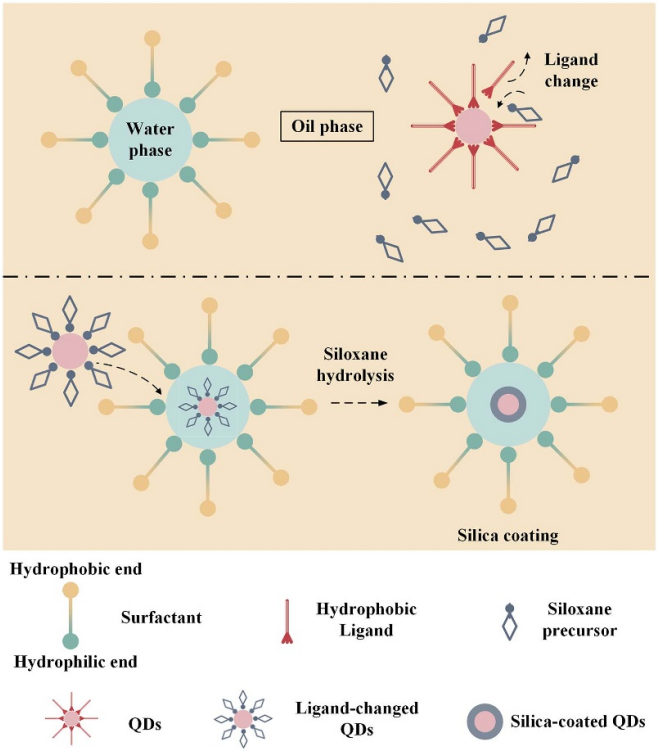

Figure 6. Microemulsion reaction process for silica-coated QDs.

the entry of QDs and siloxane precursors. Investigation on non-ionic (Brij L4 and Igepal) and anionic (AOT) surfactants showed that these surfactants caused a slight red shift of

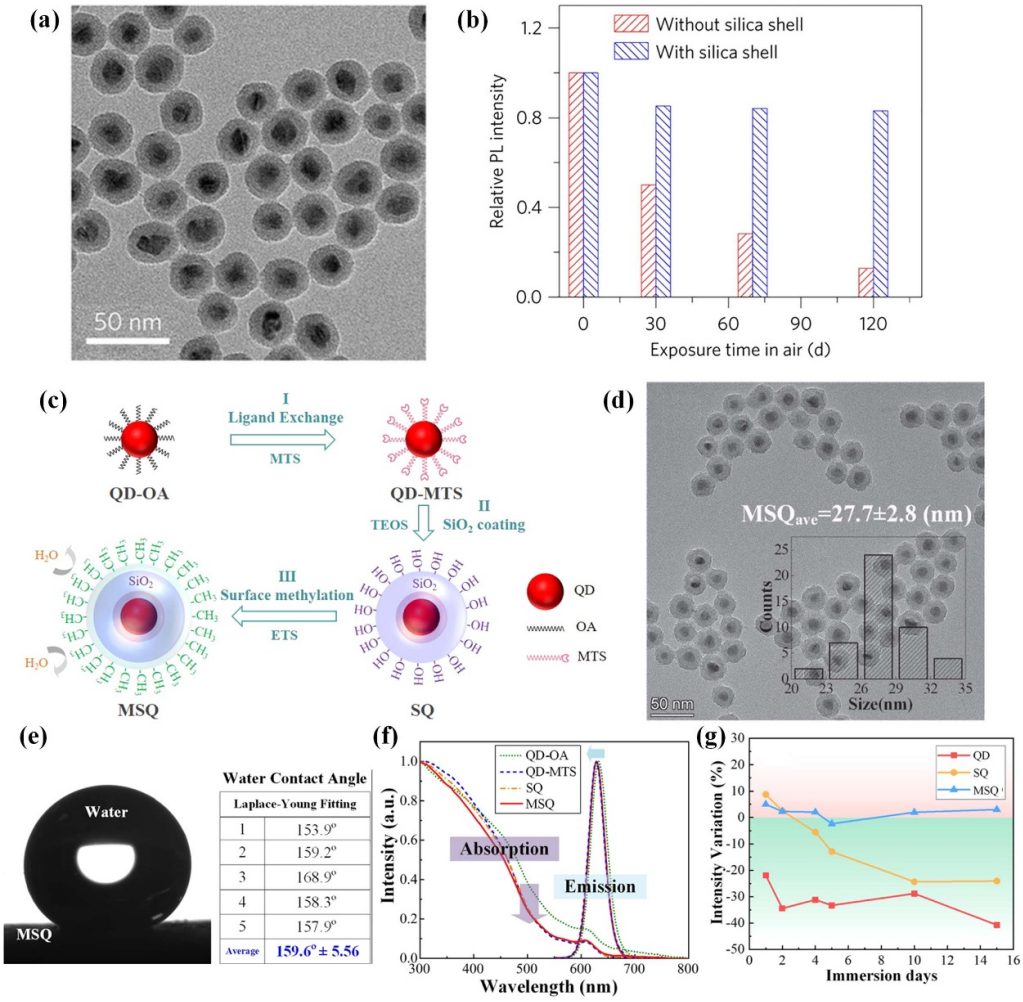

Figure 7. (a) TEM images of a large-area view of silica-coated g-QDs with mean silica-shell thickness of 5 nm. (b) PL intensity of films fabricated by silica-coated and uncoated g-QDs under different time when exposed to air and room light. Reproduced from [71], with permission from Springer Nature. (c) Schematic of the preparation process of MSQ. (d) TEM image and size distribution of MSQ. (e) PL spectra of QD, SQ and MSQ. (e) Water contact angle of MSQ. (f) Emission spectra of different samples. (g) PL intensity variation during water immersion. Reproduced from [66]. © IOP Publishing Ltd. All rights reserved.

PL spectra, a silght decrease of PLQY and a narrowing of FWHM of the QDs. Due to the anionic nature, AOT could slow down the hydrolysis of TEOS and silane polycondensation. Especially, Brij L4 stood out to be the best surfactants which formed the thickest silica shell and highest PLQY of the obtained silica-cotead QDs because it showed better interaction with the oleic acid ligands of QDs endowed by the similar linear aliphatic structure. Darbandi *et al* [68] found that QDs aggregated in very low surfactant concentration, and with increasing surfactant concentration, QD@silica nanoparticles first showed polydisperse then monodisperse. The influence of catalyst and precursors are also worthy of attention. Ammonia catalyst accelerates the hydrolysis of siloxane precursors and the rapid hydrolysis colud increase the monodispersity of silica-coated QDs. In Darbandi *et al* research, at low ammonia concentration and TEOS (siloxane precursor), irregular silica structure were built for the slow hydrolysis. As the concentration increased, polydisperse QD@silica with multiple QDs and monodisperse QD@silica with single QDs appeared in sequence. With furtherly increasing concentration of anmmonia and TEOS, irregular structures were oberserved besides relatively monodisperse QD@silica, which was attributed to the destabilization of the microemulsion. Li *et al* [71] encapsulated QDs into silica shells by microemulsion reaction. Figures 7(a) and (b) illustrates the transmission electron microscopy (TEM) images of the nanoparticles and the PL intensity of fabricated films under different time when exposed to air. The results in figure 7(b) shows that silica-coated QDs maintained ∼85% of the original PLQY after 4 month exposure to air and room light while uncoated QDs only retained ∼23%.

Nevertheless, due to the hydrophilic hydroxyl on the surface of silica shell [76], their moisture-resistant ability is weakened. Researchers proposed silica shell surface hydrophobic treatment to protect QDs more efficiently [65, 66]. Zhou *et al* [66] proposed to prepare single-dot superhydrophobic methylated core/shell silica-coated QD (MSQ). Figure 7(c) exhibits schematic of the preparation which

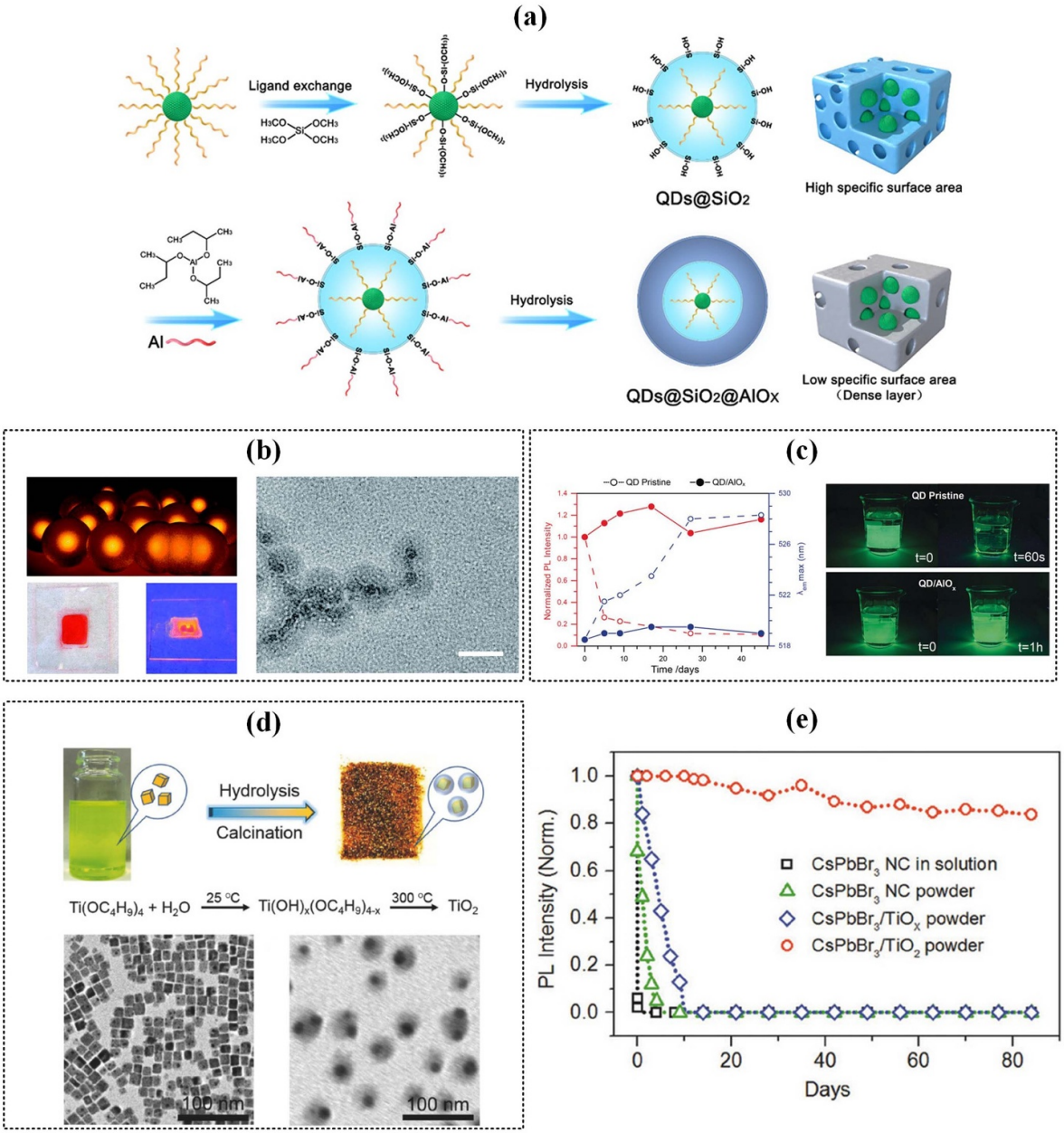

Figure 8. (a) Fabrication process of QDs@SiO_2 and QDs@SiO_2@AlO_x. Reprinted with permission from [77]. Copyright (2021) American Chemical Society. (b) Schematic of Al_2O_3-coated QDs by ALD (upper left), photograph of a drop-casted QD film under daylight and illumination by a 390 nm LED lamp (lower left), and TEM image of 20 nm Al_2O_3-coated QDs with a scale bar of 50 nm (right). Reproduced from [79] with permission from the Royal Society of Chemistry. (c) Stability comparison of QD/AlO_x film and QD film in air over 45 d and in water immersion. [80] John Wiley & Sons. [© 2017 Wiley-VCH Verlag GmbH & Co. KGaA, Weinheim. (d) Fabrication process of TiO_2-coated QDs (upper), TEM images of QDs (lower left) and TiO_2-coated QDs (lower right). (e) PL intensity of samples after immersing in Milli-Q water at different time. [82] John Wiley & Sons. [© 2017 WILEY-VCH Verlag GmbH & Co. KGaA, Weinheim].

consists of ligand exchange, SiO_2 coating and surface methylation. Figures 7(d) and (e) shows TEM images and size distributions of MSQ, and a water contact angle of 159.6° which indicated a superhydrophobic ability. Figures 7(f) and (g) give the PL spectra, and PL intensity during water immersion of QD, SiO_2 shell-coated QD (SQ) and MSQ, respectively. The results show that this coating strategy had little influence on QD's luminous characteristics. After 15 d water immersion test, PL intensity of QD and SQ dropped by 41% and 24%, while that of MSQ rose 3% for photoactivation proving the superior oxygen/moisture-resistant ability of their strategy.

Except for the above mentioned silica shell, other materials like AlO_x and TiO_2 are also adopted to coat QDs [77–82]. Yang *et al* [77] coated AlO_x layer onto QDs@SiO_2 through sol–gel method. Figure 8(a) illustrates the coating mechanism of QDs@SiO_2@AlO_x. This research showed that AlO_x possesses a denser struture with low specific surface area compared with SiO_2 proving a superior protection of AlO_x. Yin *et al* [79] used atomic layer deposition (ALD) to coat QD with

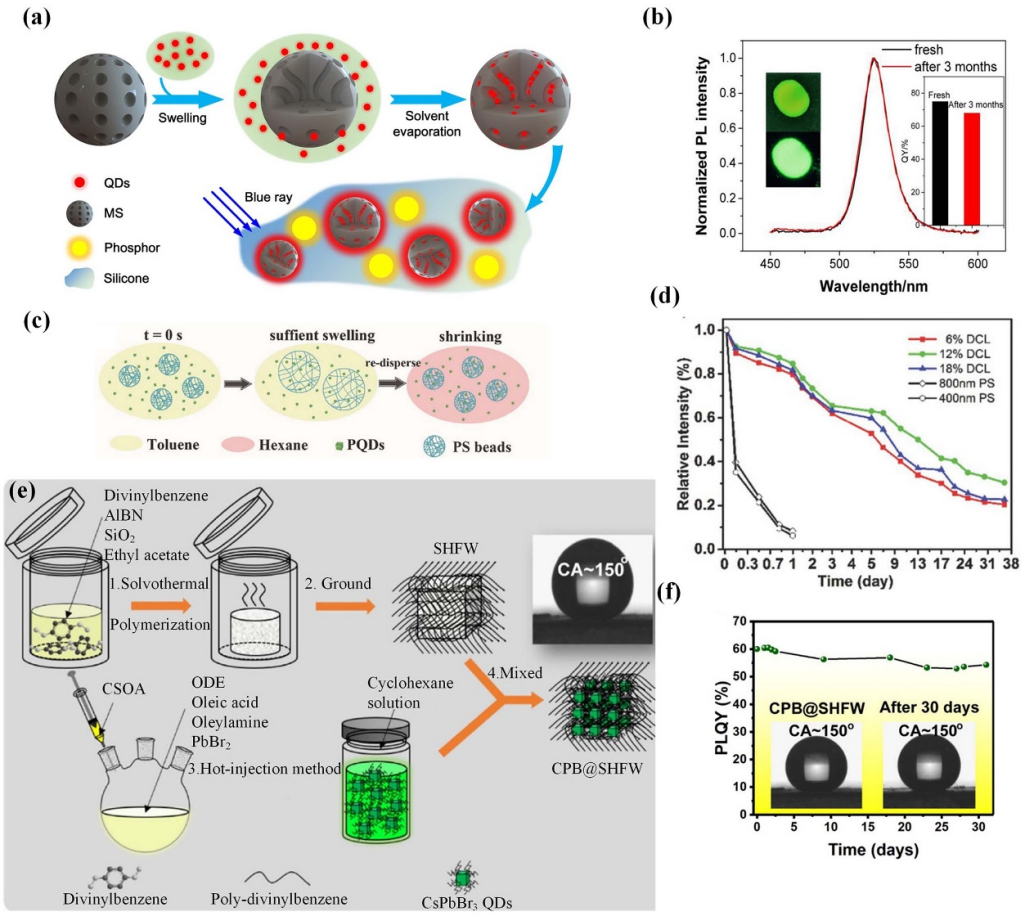

Figure 9. (a) Preparation process of QDs-LMS. Reproduced from [83]. © IOP Publishing Ltd. All rights reserved. (b) PL spectra of composite samples before and after three-month storage in wet weather. Inset in the left side shows the photograph of the aged powders under illumination of white (upper) and UV (lower) light. Inset in the right side shows the QYs of the freshly prepared and aged samples. Reprinted from [84], Copyright (2018), with permission from Elsevier. (c) Preparation process of PQDs@PS composite spheres. (d)Water resistance test of PQDs@PS composites. [85] John Wiley & Sons. [© 2017 WILEY-VCH Verlag GmbH & Co. KGaA, Weinheim]. (e) Preparation process of CPB@SHFW composites. (f) PLQY evolution of CPB@SHFW composite powders when immersed in water. Insets show the contact angle before and after being immersed in water for 31 d. Reprinted with permission from [87]. Copyright (2019) American Chemical Society.

Al_2O_3 layer. Figure 8(b) shows the schematic and images of this material. The QDs were coated with a Al_2O_3 shell with thickness of 20 nm. Loiudice *et al* [80] synthesised QDs/AlO_x by ALD and tested their stability figure 8(c) compares the stability of QD film and QD/AlO_x film in air and in water immersion. QD/AlO_x film exhibited no apparent change in both tests, while QD film suffered significant PL quenching and a red shift. Li *et al* [82] has coated QDs with TiO_2 shell and demonstrated that it could effectively suppressed anion exchange and photodegradation of QDs. Figure 8(d) illustrates the fabrication process of TiO_2-coated QDs and TEM images of QDs and TiO_2-coated QDs, where the one or two QDs were coated by a tight TiO_2 shell. Figure 8(e) gives the stability test in water. The PL intensity of TiO_2-coated QDs are extremely stable over three months while other samples were totally quenched in several days.

Incorporating QDs into mesoporous microspheres is alternative to protect QDs from the outside environment. Compared with chemically shell-coating outside QDs' surfaces, these methods physically absorbe QDs into mesoporous microspheres in a much more mild system [83–87]. Figure 9(a) exhibits the preparation of QDs-luminescent mesoporous silica (QDs-LMS) in the work of Xie *et al* [83]. They adopted swelling and evaporation method to allow QDs to enter into the pores of mesoporous silica, where oxygen and moisture molecules permeat slower than in polymer matrix. Su *et al* [84] incorporated QDs into meoporous silica with pore size of 15 nm. After a storage in wet weather with relative humidity of 70% ± 5% for three months, the composite powders still preserved 90% of its initial QY, as shown in figure 9(b). Besides commonly used mesoporous silica, Wei *et al* [85] proposed to prepare perovskite QDs@polystyrene (PQDs@PS) nano/micron composite beads via a simple swelling–shrinking strategy. Figure 9(c) illustrates the schematic of PQDs@PS's preparation process. Crosslinked PS first swelled in good solvent (toluene) solved with PQDs to incorporated PQDs into its network. Then PQDs@PS was tranfered to theta solvent (hexane) solved with PQDs in the same concentration, where the swelled PS shrinked to realize a compact encapsulation of PQDs. In figure 9(d), the water resistance test shows that

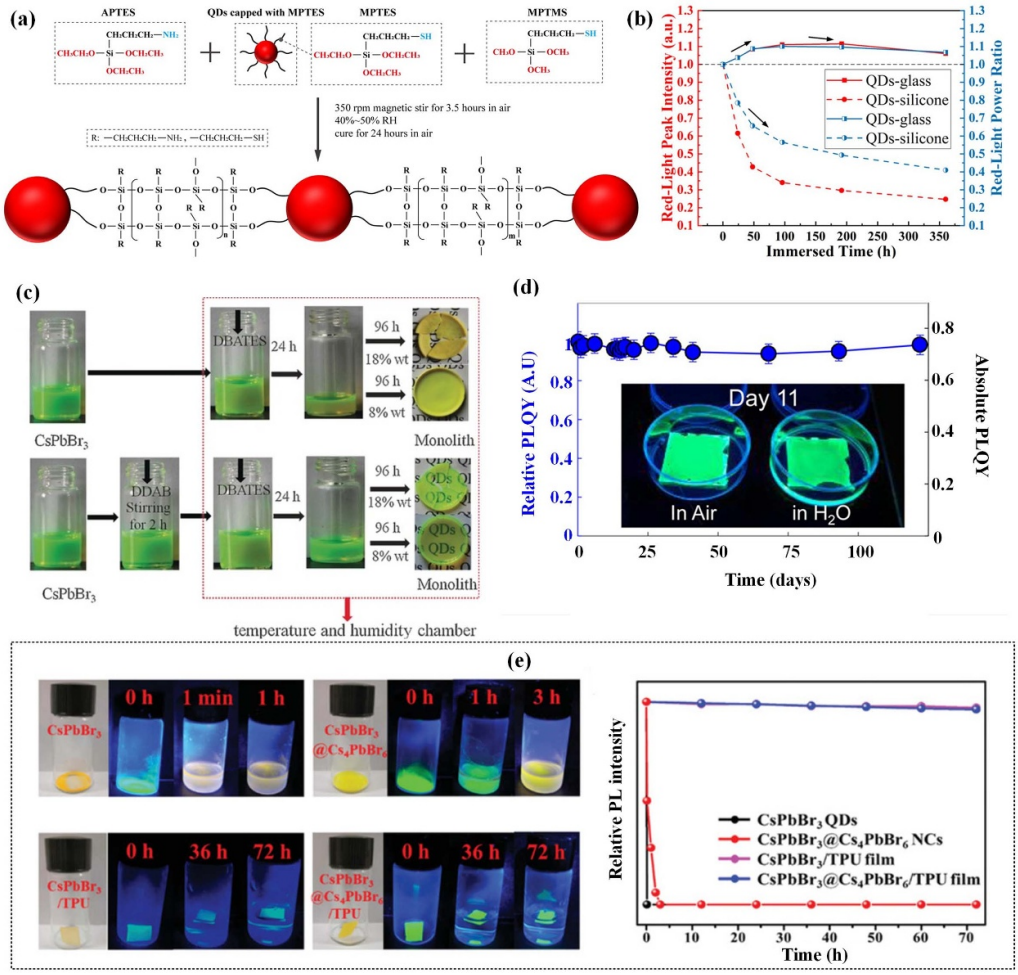

Figure 10. (a) Schematic of the fabrication process of QDs-glass. (b) PL performances of QDs-glass and QDs-silicone after different immersed time. Reproduced from [32]. © IOP Publishing Ltd. All rights reserved. (c) Photographs of $CsPbBr_3$ QDs, DDAB treated QDs, solution after adding DBATES into QDs solutions and their corresponding monolith with different content of QDs. [93] John Wiley & Sons. [© 2017 Wiley-VCH Verlag GmbH & Co. KGaA, Weinheim]. (d) Relative and absolute QY of QDs-polymer composite films over four months of water soaking. Reprinted with permission from [88]. Copyright (2016) American Chemical Society. (e) Photographs (left) and the PL intensity (right) of the samples immersed in water. [94] John Wiley & Sons. [© 2019 WILEY-VCH Verlag GmbH & Co. KGaA, Weinheim].

the composites exhibited excellent water-resistant ability. The composites still retained 20%–30% PL intensity after 30 d of stirring in water. Superhydrophobic framworks were carried out by Xuan *et al* [87]. They obtained superhydrophobic POP frameworks (SHFW) and absorbed QDs into them forming surperhydrophobic composites (Details are shown in figure 9(e)). The superhydrophobic composites exhibited a water contact angle of 150°, which protected the QDs for a month even being immersed in water as the PLQY evolution shown in figure 9(f).

3.2. Novel packaging matrix

Some novel matrixes for packaging are developed to take the place of conventional polymer matrix with a much lower oxygen/moisture permeation coefficient. Compared with the micro–nano buffer layer, the packaing matrix builds low-permeating ways in the whole package rather than only in a micro-scale shell. This strategy possesses stronger protection theoretically but the application is limited in some cases because it is not so flexible in use as the micro-scale shells. In addition, the compatibility between the matrix and QDs are highly required to maintain the characteristics of QDs [88].

Silica is used not only as a nano-scale shell outside QDs, but as a packaging matrix [32, 64, 89–92]. Kim *et al* [89] fabricated QD/siloxane (methacryl) film which had chemical linkages between matrix and QD. They reported that chemical linkages are benefical to QD's PLQY and moisture stability by producing effective siloxane passivation layer intact on the QD's surface. Alternatively, reserachers also exchanged the surface ligands of QDs by siloxane to build a chemical linkage between QDs and silica matrix [32, 90, 92]. As shown in figure 10(a), Yang *et al* [32] fabricated densely cross-linked QDs-glass by utilizing 3-mercaptopropyl triethoxysilane (MPTES) capped QDs, and siloxane precursors with short chain [3-mercaptopropyl trimethoxysilane (MPTMS)

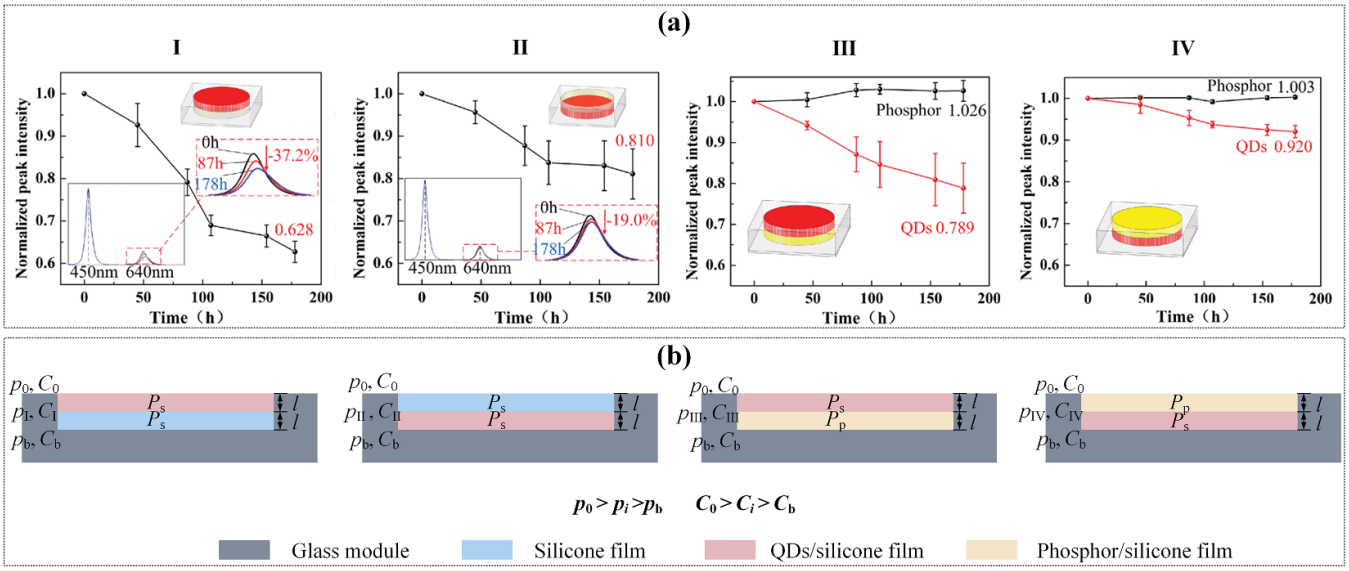

Figure 11. (a) Time evolution of normalized light peak intensity of QDs/silicone film (I) upon and (II) below silicone film, and QDs/silicone film (III) upon and (IV) below phosphor film. Insets are the corresponding packaging structures. © [2020] IEEE. Reprinted, with permission, from [98]. (b) Permeation models of the layered packaging structures.

and 3-aminopropyl trimethoxysilane (APTES))]. Caculated by Brunauer–Emmett–Teller method, the silica glass showed a 68.6% lower cumulative pore volume than silicone, which proved its denser structure. Figure 10(b) gives the PL characteristics of QDs-glass and QDs-silicone during the water immersion test. After 360 h water immersion, QDs-glass maintained its PL intesity while QDs-silicone reduced to 24.7% of the initial. Furtherly, Li *et al* [93] obtained a robust QDs-SiO_2/Al_2O_3 monolith with remarkable stability and PLQY (90%) by Di-sec-butoxyaluminoxytriethoxysilane (DBATES), as illustrated in figure 10(c). The authors exchanged the surface ligand of QDs by diodecyl dimethyl ammonium bromide (DDAB) to stable the QDs in the matrix, which enhanced the PLQY up to 90%.

Non-silica type novel packaing matrix are also developed by researchers in recent years. Raja *et al* [88] adopted poly(styrene–ethylene–butylene–styrene) (SEBS) which contains alkyl chain ligands with chemically silimilar composition to the native alkyl chain ligands (oleyamine and oleic acid) on the QDs surface. In this way, a strong QD-polymer interface matching was created which minimizes ligand loss during encapsulation and suppresses oxygen/moisture molecules diffusion to QDs surface [95–97]. As shown in figure 10(d), after 122 d water soaking test, QDs-polymer exhibited no change on the realtive and absolute QY. In study of Shi *et al* [94], a thermoplastic polyurethane (TPU) encapsulation strategy under room temperature was proposed to improve QDs' properties of oxygen/moisture resistance. The results in figure 10(e) demonstrated that the PL intensity of TPU encapsulated QDs film was very stable after immersed in water for 72 h.

3.3. Novel packaging structures

Since oxygen and moisture molecules permeat through the entire packaging of QDs converted optoelectronic devices, optimization of packaging structre is necessary to enhance moisture resistance.

Pei *et al* [98] investigated the moisture stability of QDs-LEDs with layered packaging structures. Figure 11(a) shows the time evolution of normalized red light peak intensity in a high moisture environment with relative humidty of ~99.8% and temperature of 50 °C, and the corresponding packaging structures. After 178 h aging, the normalized red light peak intensity remained 0.789 of structure I, 0.920 of structure II, 0.628 of structure III, and 0.810 of structure IV. The structure that QDs/silicone film in the lower layer exhibited higher red light peak intensity and the structure with phosphor/silicone layer in the upper layer was better than silicone. We revealed the mechanism utlizing the theories in section 2, and the corresponding models are shown in figure 11(b). The totall permeation coefficent P_i (i is stand for I, II, III and IV) of four structures are calculated by equation (6) as follows:

$$P_i = \frac{P_U + P_L}{2} \tag{19}$$

where P_U and P_L are the permeation coefficient of the upper layer and lower layer, respectively. P_s is the permeation coefficient of silicone. Due to the small size and low volume fraction of QDs, the permeation coefficient of QDs/silicone film is nearly equal to P_s. The phosphor/silicone film's permeation coefficient P_p can be calculated by equation (8), which is smaller than P_s. The pressure of the interface p_i is calculated by equation (4) by considering that the mass transfer rate of the whole structure is equal to the upper layer:

$$p_i = 0.75p_0 + 0.25p_b - 0.25\frac{P_L}{P_U}(p_0 - p_b) \tag{20}$$

where p_0 and p_b are the partial pressure of oxygen/moisture on the top and bottom surfaces. The calculation results of the

Table 1. Permeation coefficient P_i, interface pressure p_i and interface concentration C_i for the four packaging structures.

Structure	P_i	p_i
I	P_s	$0.5\ p_0 + 0.5p_b$
II	P_s	$0.5\ p_0 + 0.5p_b$
III	$(P_s + P_p)/2$	$0.75\ p_0 + 0.25p_b$_$0.25P_p/P_s(p_0 - p_b)$
VI	$(P_s + P_p)/2$	$0.75\ p_0 + 0.25p_b$_$0.25\ P_s/P_p(p_0 - p_b)$

Table 2. Expression of C_i, C_u and C_b of the four structures.

Structure	C_i	C_u	C_b
I	S_0p_I	S_0p_0	S_0p_I
II	S_0p_{II}	S_0p_{II}	S_0p_b
III	S_0p_{III}	S_0p_0	S_0p_{III}
VI	S_0p_{IV}	S_0p_{IV}	S_0p_b

four structures are listed in table 1. Considering that P_p/P_s is smaller than unit, thus $P_{IV} = P_{III} > P_{II} = P_I$, which explains that red light peak intensity of structure III is higher than structure I, and structure IV is higher than strucure II after aging. Then we furtherly investigated the mechanism of the effect of QDs/sillicone's location on the performances. The concentration of oxygen/moisture in the interface C_i is calculated by equation (1) and listed in table 2.The solubilities of silicone, QDs/silicone and phosphor/silicone film are taken as the same as S_0. The concentration distribution of QDs/silicone film at time t before steady state is derived from equation (3) as:

$$C_i(x) = \frac{C_u - C_b}{l}x + C_b \tag{21}$$

and the average concentration C_{mi} of QDs/silicone film is:

$$\begin{aligned} C_{mi} &= \frac{\int_{C_b}^{C_u} C_i(x)\,\mathrm{d}x}{\int_0^l \mathrm{d}x} \\ &= \frac{C_u + C_b}{2}\cdot\frac{(C_u - C_b)^2}{l^2} + C_b\cdot\frac{C_u - C_b}{l} \\ &= \Delta\bar{C}_i^2\bar{C}_i + C_b\Delta\bar{C}_i \end{aligned} \tag{22}$$

$$\Delta\bar{C}_i = \frac{C_u - C_b}{l}, \bar{C}_i = \frac{C_u + C_b}{2} \tag{23}$$

where C_u and C_b are the concentration in the upper and bottom surfaces of QDs/silicone film, respectively, l is the thickness of the QDs/silicone film. $\Delta\bar{C}_i$ is concentration gradient and $\bar{C}_i$ is mean value of concentration in the upper and bottom surfaces. The expression of C_u and C_b of different structures are listed in table 2. According to p_i in table 1, it can be found that there is $S_0p_{III} > S_0p_{II} = S_0p_I > S_0p_{IV}$. Therefore, the relationship of $\Delta\bar{C}_i$ is $\Delta\bar{C}_{III} > \Delta\bar{C}_{II} = \Delta\bar{C}_I > \Delta\bar{C}_{IV}$ and $\bar{C}_i$is $\bar{C}_{III} > \bar{C}_I > \bar{C}_{II} > \bar{C}_{IV}$. The above relationships determine that $C_{mIII} > C_{mI} > C_{mII} > C_{mIV}$. A lower oxygen/moisture concentration explains the higher red peak intensity of the structures with QDs/silicone film in the lower layer than the upper ones after aging. Due to the lowest permation coefficient and average concentation of structure IV, it showed the highest stability among the four structures in the aging test.

The above analysis revealed that the key to enhance oxygen/moisture resistance is reducing the total permeation coefficient and the oxygen/moisture concentration on the surfaces.

Ji *et al* [99] proposed a multilayer coextruded QD diffuser plate for QDs' stability improvement. By sandwiching QDs layer between PMMA layers, the oxygen/moisture concentration on the upper and lower surfaces were reduced. The QDs were first coated with a SiO_2 coating layer, and then the multilayer structure was fabricated by a self-developed multilayer coextrusion molding equipment as figure 12(a) illustrates. The three layers are molded and extruded into a complete QD diffuser plate by means of a roller with a microtemplate at the outlet of the extruder. The QDs disperse in the middle functional layer for colour conversion, while the upper and lower PMMA diffuser layers isolate the ambient oxygen and moisture to protect QDs, and mix and homogenize the light. Figure 12(b) gives the brightness decay of the samples with different PMMA layer thickness at 85 °C and 85% RH for over 2000 h. As the PMMA thickness increased, the brightness decay decreased for the lower surface oxygen/moisture concentration according to equation (21). Yu *et al* [100] treated the surface of QDs-LEDs with superhydrophobic nanosilica (NS) particles. The superhydrophobic surface reduced the moisture concentration of QDs/polymer film upper surface. Figure 12(c) exhibits the synthesis process of 1 H, 1 H, 2 H, 2 H-perfluorooctyltrichlorosilane (FOTS) modified NS particles. Then FOTS-NS were coated on the surface of phosphor (QDs)/polymer film of QDs-LEDs as shown in figure 12(d). After aging for 270 h, the normalized peak intensity degradation of QDs embedded in the coated and uncoated films is ∼35.68% (blue line) and ∼77.66% (red line) as shown in figure 12(e).

Yang *et al* [101] used bidirectional stretching force field to stretch and extend organic barrier phase EVOH into a flake structure which was oriented along the extrusion direction to fabricate multilayer QD diffusion plate (QD-DP). Figure 12(f) shows the fabrication process and the schematic of the layer-by-layer structure. From the structure in figure 12(f), the dispersed impermeable EVOH sheets in the methyl methacrylate–styrene copolymer (MS) matrix prolonged the permeating pathway of oxygen and moisture molecules thus reducing the total permeation coefficient and protecting QDs. They fabricated pure MS layer and QD-doped MS (MS-QD) layer alternating multi-layer materials (MS/MS-QD) with 128 layers, and EVOH sheets-doped MS (MS-E) layer and MS-QD layer alternating multi-layer materials (MS-E/MS-QD) with 128 layers. Figures 12(g) and (h) compared the spectra of MS/MS-QD and MS-E/MS-QD 128 layers after 512 h thermal-oxygen process under 80 °C. The results show that the time of fluorescence intensity decreased by 10% of MS-E/MS-QD is 512 h which is 4.7 times longer than that of MS/MS-QD (108 h).

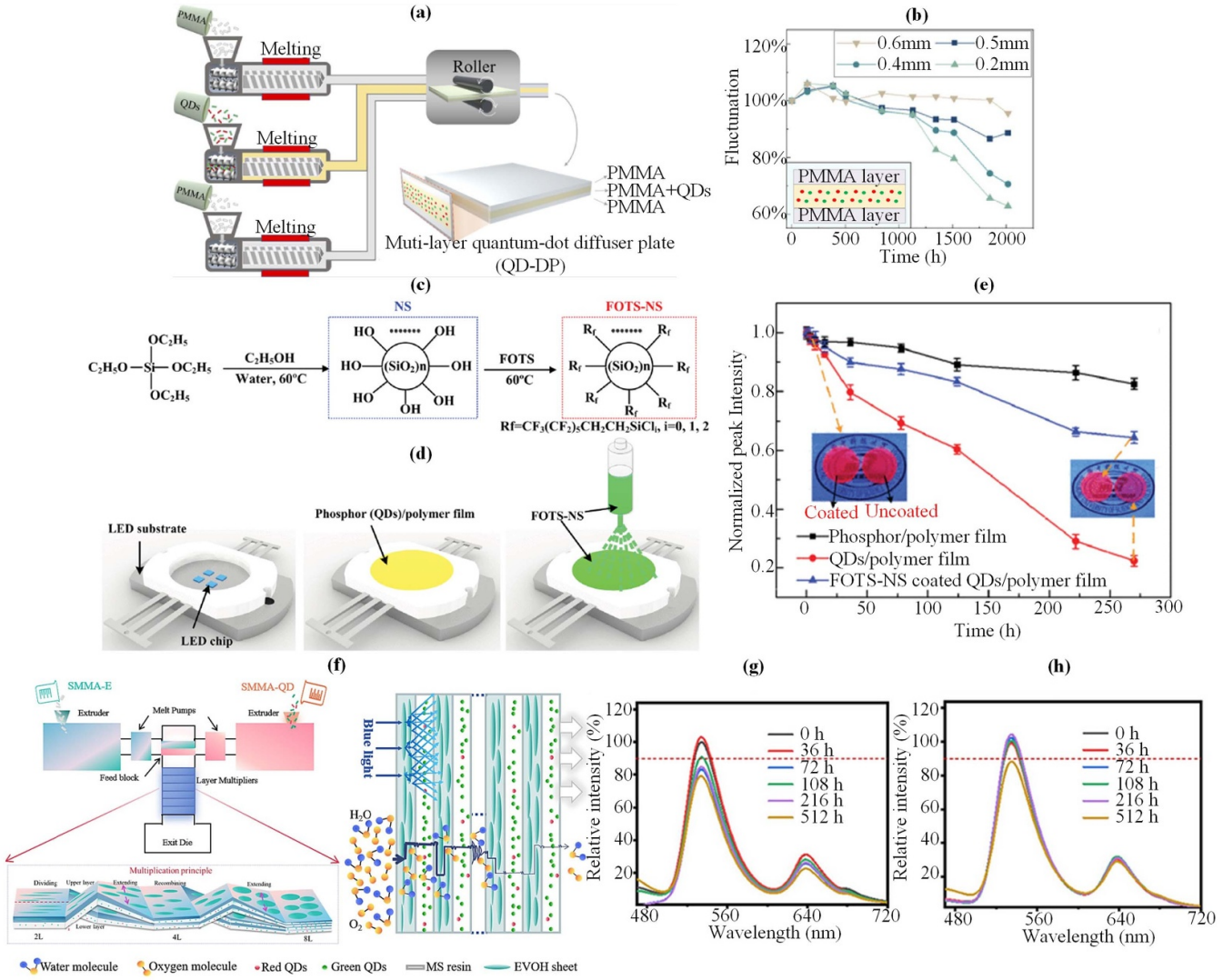

Figure 12. (a) Multilayer coextrusion method. (b) Brightness decay of QD diffuser plates with different PMMA layer thickness at 85 °C and 85% RH for over 2000 h. Reproduced from [99]. CC BY 4.0. (c) Synthesis process of the superhydrophobic NS particles. (d) Fabrication process of FOTS-NS-coated LEDs. (e) Time evolution of the normalized peak intensity of phosphor/polymer film, QDs/polymer film and FOTS-NS coated QDs/polymer film. © [2019] IEEE. Reprinted, with permission, from [100]. (f) Fabrication process of multilayer QD diffusion plate and schematic of the layer-by-layer structure. Fluorescence spectra of QD-DP of (g) MS/MS-QD 128 layers, and (h) MS-E/MS-QD 128 layers before and after thermal-oxygen process. Reprinted from [101], Copyright (2024), with permission from Elsevier.

Table 3 summarizes the strategies for packaging-inside oxygen/moisture-resistance of micro–nano buffer layer, novel packaing matrix and novel packaing structure.

4. Summary and outlook

In this review, we first introduce the oxygen/moisture-induced degradation mechanism on QDs. Then we discuss permeation models under different circumstances, including homogenous/inhomogeous polymer, and temperature-dependent permeation. Finally, we devide the promising oxygen/moisture-resistant strategies for QDs optoelectronic devices into three categories from a packaging perspective, and analyze them with permeation theory. Based on these state-of-the-art advances, we image the future directions of this field.

First, in this review, the most of the strategies for resisting oxygen/moisture rely solely on qualitative analysis. Researchers have developed multitudinous experimental methods to enhance and optimize the oxygen/moisture resistance, which worked well but was costly and ineffective. From a packaging perspective, current strategies are still insufficient to theoretically design and optimize the packaging structures. The absence of precise permeation model is the main reason. Combining the existing experimental methods with theoretical models would significantly improve the efficiency and precision. However, there still needs a lot of efforts to achieve a precise permeation model, such as reliable measurement of oxygen/moisture concentration, permeation coefficient, diffusion coefficient and solubility, especially in inhomogeneous polymers, multilayer structures and temperature-varying conditions.

Table 3. Packaging-inside oxygen/moisture-resistant strategies.

Strategy	Method	Material	Test	Performance	Year
Micro–nano buffer layer	Silica coating	TEOS, NH_4OH, and IGEPAL CO-520	Four month exposure to air and room light	QY retain 85% of the initial	2016 [71]
	Silica coating	TEOS and MPTMS	Aging at 85 °C and 5% RH	PLQY decreased by 13%	2019 [64]
	Silica coating	TMOS and ammonia	Aging in a mixture of toluene and water (4:1)	PL intensity remained 59.6%	2020 [73]
	Silica coating	Carboxylate and SiO_2	Packaged LEDs continuous operated at 5 mA–38% RH in air	Light intensity remained 85%	2021 [62]
	Silica coating	TMOS and toluene	Packeged LEDs operated at 100 mA for 20 d	Luminous intensity remain 69.3%	2021 [72]
	Silica coating	TMOS and tolune	405 nm blue laser at 0.31 W cm^{-2}, air with 30%–40% RH, 80 °C	No fluorescent quenching	2021 [74]
	Silica coating with QDs capped by APTES	APTES	Left in air at room temperature for 3 months	PLQY droped by 5%	2016 [63]
	Superhydrophobic silica coating	MPTMS, ethoxy trimethyl silane (ETS) and TEOS	Immersed in water for 15 d	PL intensity rose by 3%	2022 [66]
	AlO coating	Trimethylaluminum (TMA) and water	Storage under ambient enviroment for 45 d	No apparent change appeared	2017 [80]
	AlO coating	*Sec*-butoxide and *tert*-butyl alcohol	Illuminated by blue LED chip at 20 mA under 70% RH for 1080 h	Light conversion efficiency decreased by 37%	2021 [77]
	TiO_2 coating	$Ti(OC_4H_9)_4$	Immersed in Milli-Q water for three months	PL intensity remained ∼80%	2017 [82]
	Mesoporous silica absorption	Meso-SiO_2	Storage in wet weather with 70% RH for 3 months	QY preserved 90% of the initial	2018 [84]
	Polystyrene beads encapsulation	Polystyrene beads	Stirring in water	PL intensity retained 20%–30%	2017 [85]
	Super-hydrophobic porous organic polymer frame works	Divinylbenzene, AlBN, SiO_2, and ethyl acetate	Immersed in water for 31 d	PLQY maintained at 91% of the initial	2019 [87]
Novel packaging matrix	Silica glass	TEOS and MPTMS	Illuminated by LEDs at 350 mA	Emission intensity remained 90%	2013 [92]
	Silica glass	APTES, MPTMS,and MPTES	Immersed in water for 360 h	PL intensity rose 6%	2022 [32]
	SiO_2/Al_2O_3 monolith	DBATES and DDAB	Illuminated by a LED for 300 h	PL intensity remained 90%	2017 [93]
	Maroscale polymer	SEBS	Water-soaking for 122 d	No change on QY	2016 [88]
	TPU encapsulation	TPU	Immersed in water for 72 h	No change on PL intensity	2019 [94]

(Continued.)

Table 3. (Continued.)

Novel packaging structures	Layered packaging with QDs layer encapsulated in the lower layer	Silicone	Aged at 50 °C and 99.8% RH for 178 h	PL intensity remained 92%	2020 [98]
	Multi-layer co-extruded QDs diffuser plate	PMMA	Tested at 85 °C and 85% RH for 2000 h	Bright fluctuation is lower than 10%	2022 [99]
	Superhydrophobic coating on the surface	FOTS	Aged at 50 °C and 99.6% RH for 270 h	PL intensity remained 77.66%	2019 [100]
	QD diffusion plate incoporated with flake EVOH	EVOH and MS	Thermal-oxygen aged at 80 °C for 512 h	Fluorescence decreased by 10%	2024 [101]

Second, from section 2.2.3, it can be seen that the rising temperature results in a remarkable enhancement on the diffusion of oxygen/moisture molecules in polymers. During the operation of QDs converted devices, the temperature rise could exceed 100 °C [102], which promotes the diffusion within the packaging. Therefore, temperature control is also important in resisting oxygen/moisture. High thermal-conductive fillers such as hexagonal boron nitride are utilized in thermal management of QDs converted devices [52, 103–105]. Especially, most of the thermal-conductive fillers are impermeable which is beneficial to oxygen/moisture resistance according to equation (8). Adopting appropriate alignment engineering of the fillers [106] can simultaneously maximize the effect of thermal management and oxygen/moisture resistance.

Third, with the rapid development of optoelectronic devices, requirements on the reliability are sharply increasing. The unitary resisting strategies may become insufficient in the future. Therefore, new strategies for oxygen and moisture molecules absorption and elimination are promising in this field. However, the challenges of this kind of strategy could be the compatibility with QDs and the influence on luminous ability.

Data availability statement

All data that support the findings of this study are included within the article (and any supplementary files).

Acknowledgments

This work is supported by the National Natural Science Foundation of China (52106089).

ORCID iDs

Bin Xie https://orcid.org/0000-0001-9031-5900
Xiaobing Luo https://orcid.org/0000-0002-6423-9868

References

[1] Li Y, Deng M, Zhang X, Qian L and Xiang C 2024 *Nano-Micro Lett.* **16** 105
[2] Shi Y, Zhang Y, Wang Z, Yuan T, Meng T, Li Y, Li X, Yuan F, Tan Z A and Fan L 2024 *Nat. Commun.* **15** 3043
[3] Li X *et al* 2023 *BMEMat* **1** 12045
[4] Wang J, Zhu Y and Wang L 2019 *Chem. Rec.* **19** 2083–94
[5] Aftab S, Iqbal M Z, Hussain S, Kabir F, Al-Kahtani A A and Hegazy H H 2023 *Adv. Funct. Mater.* **33** 2303449
[6] Chen J, Jia D, Zhuang R, Hua Y and Zhang X 2023 *Adv. Mater.* **36** 2306854
[7] Liu B *et al* 2024 *Adv. Funct. Mater.* **34** 2401007
[8] Wang Y, Ta V D, Leck K S, Tan B H I, Wang Z, He T, Ohl C-D, Demir H V and Sun H 2017 *Nano Lett.* **17** 2640–6
[9] Wu Y, Cai W, Huang Z, Ren Y, Wu Y and Wang Y 2024 *Laser Photon. Rev.* **18** 2301167
[10] Ji Y *et al* 2024 *ACS Nano* **18** 8157–67
[11] Jiang J, Zhang S, Shan Q, Yang L, Ren J, Wang Y, Jeon S, Xiang H and Zeng H 2024 *Adv. Mater.* **36** 2304772
[12] Li Y *et al* 2024 *Nano Lett.* **24** 3237–42
[13] Fan X *et al* 2023 *Adv. Mater.* **35** 2300834
[14] Kang C, Prodanov M F, Gao Y, Mallem K, Yuan Z, Vashchenko V V and Srivastava A K 2021 *Adv. Mater.* **33** 2104685
[15] Kim J, Roh J, Park M and Lee C 2023 *Adv. Mater.* **36** 2212220
[16] Kim D, Yun T, An S and Lee C-L 2024 *Nano Converg.* **11** 4
[17] Samiei S, Soheyli E, Vighnesh K, Nabiyouni G and Rogach A L 2023 *Small* **20** 2307972
[18] Wang Y, Ding G, Mao J Y, Zhou Y and Han S T 2020 *Sci. Technol. Adv. Mater.* **21** 278–302
[19] Moon H, Lee C, Lee W, Kim J and Chae H 2019 *Adv. Mater.* **31** 1804294
[20] Hu Z, Shu Y, Qin H, Hu X and Peng X 2021 *J. Am. Chem. Soc.* **143** 18721–32
[21] Huang S, Li Z, Wang B, Zhu N, Zhang C, Kong L, Zhang Q, Shan A and Li L 2017 *ACS Appl. Mater. Interfaces* **9** 7249–58
[22] Ko J *et al* 2020 *NPG Asia Mater.* **12** 19
[23] Carrillo-Carrión C, Cárdenas S, Simonet B M and Valcárcel M 2009 *Chem. Commun.* 5214–26
[24] Cordero S, Carson P, Estabrook R, Strouse G and Buratto S 2000 *J. Phys. Chem.* B **104** 12137–42
[25] Jones M, Nedeljkovic J, J, Ellingson R J, Nozik A and Rumbles G 2003 *J. Phys. Chem.* B **107** 11346–52
[26] Pechstedt K, Whittle T, Baumberg J and Melvin T 2010 *J. Phys. Chem.* C **114** 12069–77
[27] Paydary P and Larese-Casanova P 2020 *J. Environ. Sci.* **90** 216–33
[28] van Sark W G J H M, Frederix P L T M, Bol A A, Gerritsen H C and Meijerink A 2002 *ChemPhysChem* **3** 871–9
[29] Wang Y, Tang Z, Correa-Duarte M A, Liz-marza´n Luis M and Kotov N A 2003 *J. Am. Chem. Soc.* **125** 2830–1
[30] Wang Y, Tang Z, Correa-Duarte M A, Pastoriza-Santos I, Giersig M, Kotov N A and Liz-marza´n L M 2004 *J. Phys. Chem.* B **108** 15461–9

[31] Dembski S, Graf C, Krüger T, Gbureck U, Ewald A, Bock A and Rühl E 2008 *Small* **4** 1516–26
[32] Yang X, Zhou S, Zhang X, Xiang L, Xie B and Luo X 2022 *Nanotechnology* **33** 465202
[33] Wijmans J 2004 *J. Membr. Sci.* **237** 39–50
[34] Crank J 1975 *The Mathematics of Diffusion* (Oxford University Press)
[35] Kalnin J R and Kotomin E 1998 *J. Phys. A: Math. Gen.* **31** 7227–34
[36] De Sitter K, Winberg P, D'Haen J, Dotremont C, Leysen R, Martens J A, Mullens S, Maurer F H J and Vankelecom I F J 2006 *J. Membr. Sci.* **278** 83–91
[37] Lue S, Lee D, Chen J, Chiu C, Hu C, Jean Y and Lai J 2008 *J. Membr. Sci.* **325** 831–9
[38] Zarabadipoor M, Maghami S, Mehrabani-Zeinabad A and Sadeghi M 2021 *Comput. Mater. Sci.* **197** 110590
[39] Visweswaran B, Mandlik P, Mohan S H, Silvernail J A, Ma R, Sturm J C and Wagner S 2015 *J. Vac. Sci. Technol.* A **33** 031513
[40] Sato S, Suzuki M, Kanehashi S and Nagai K 2010 *J. Membr. Sci.* **360** 352–62
[41] Merkel T, Freeman B, Spontak R, He Z, Pinnau I, Meakin P and Hill A 2002 *Science* **296** 519–22
[42] Gonzo E, Parentis M and Gottifredi J 2006 *J. Membr. Sci.* **277** 46–54
[43] Higuchi W I 1958 *J. Phys. Chem.* **62** 649–53
[44] Lewis T B and Nielsen L E 2003 *J. Appl. Polym. Sci.* **14** 1449–71
[45] Nielsen L E 2003 *J. Appl. Polym. Sci.* **17** 3819–20
[46] Merkel T, He Z, Pinnau I, Freeman B, Meakin P and Hill A 2003 *Macromolecules* **36** 6844–55
[47] Aroon M A, Ismail A F, Matsuura T and Montazer-Rahmati M M 2010 *Sep. Purif. Technol.* **75** 229–42
[48] Maghami S, Sadeghi M and Mehrabani-Zeinabad A 2017 *Polym. Test.* **63** 25–37
[49] Vinh-Thang H and Kaliaguine S 2013 *Chem. Rev.* **113** 4980–5028
[50] Mahajan R and Koros W J 2002 *Polym. Eng. Sci.* **42** 1432–41
[51] Mahajan R and Koros W J 2002 *Polym. Eng. Sci.* **42** 1420–31
[52] Xie B, Wang Y, Liu H, Ma J, Zhou S, Yu X, Lan W, Wang K, Hu R and Luo X 2022 *Chem. Eng. J.* **427** 130958
[53] Maghami S, Mehrabani-Zeinabad A, Sadeghi M, Sánchez-Laínez J, Zornoza B, Téllez C and Coronas J 2019 *Chem. Eng. Sci.* **205** 58–73
[54] Rabiee H, Soltanieh M, Mousavi S A and Ghadimi A 2014 *J. Membr. Sci.* **469** 43–58
[55] Dadaniya A and Datla N V 2019 *Sol. Energy Mater. Sol. Cells* **201** 110063
[56] Safari M, Ghanizadeh A and Montazer-Rahmati M M 2009 *Int. J. Greenhouse Gas Control* **3** 3–10
[57] Ahmadpour E, Sarfaraz M V, Behbahani R M, Shamsabadi A A and Aghajani M 2016 *J. Nat. Gas Sci. Eng.* **35** 33–41
[58] Hülsmann P, Weiß K A and Köhl M 2012 *Prog. Photovolt., Res. Appl.* **22** 415–21
[59] Dadaniya A and Datla N V 2020 *IEEE J. Photovolt.* **10** 306–14
[60] Lita A, Washington A L, van de Burgt L, Strouse G F and Stiegman A E 2010 *Adv. Mater.* **22** 3987–91
[61] Kobayashi Y, Nozawa T, Nakagawa T, Gonda K, Takeda M, Ohuchi N and Kasuya A 2010 *J. Sol-Ge Sci. Technol.* **55** 79–85
[62] Liu Y, Zhang L, Long X, Jiang P, Geng C and Xu S 2021 *J. Mater. Chem.* C **9** 12581–9
[63] Sun C, Zhang Y, Ruan C, Yin C, Wang X, Wang Y and Yu W W 2016 *Adv. Mater.* **28** 10088–94
[64] Kim Y H, Lee H, Kang S M and Bae B S 2019 *ACS Appl. Mater. Interfaces* **11** 22801–8
[65] Tu S, Yin Q, Shang B, Chen M and Wu L 2019 *Chem. Asian J.* **14** 3830–4
[66] Zhou S, Xie B, Yang X, Zhang X and Luo X 2022 *Nanotechnology* **33** 195202
[67] Goftman V V, Aubert T, Ginste D V, Van Deun R, Beloglazova N V, Hens Z, De Saeger S and Goryacheva I Y 2016 *Biosens. Bioelectron.* **79** 476–81
[68] Darbandi M, Thomann R and Nann T 2005 *Chem. Mater.* **17** 5720–5
[69] Wang S, Li C, Yang P, Ando M and Murase N 2012 Colloids and Surf. A **395** 24–31
[70] Goryacheva O A, Wegner K D, Sobolev A M, Hausler I, Gaponik N, Goryacheva I Y and Resch-Genger U 2022 *Anal. Bioanal. Chem.* **414** 4427–39
[71] Li H, Wu K, Lim J, Song H-J and Klimov V I 2016 *Nat. Energy* **1** 16157
[72] Liu Z, Li F, Huang G, Zhao F, Zhang W, Jiang G, Cheng S, Fang Z, Zhu Q and Huang Y 2021 *J. Alloys Compd.* **888** 161505
[73] Wang B, Zhang S, Liu B, Li J, Cao B and Liu Z 2020 *ACS Appl. Nano Mater.* **3** 3019–27
[74] Zhang L, Xie Y, Tian Z, Liu Y, Geng C and Xu S 2021 *ACS Appl. Mater. Interfaces* **13** 30076–85
[75] Xie B, Liu H, Sun X W, Yu X, Wu R, Wang K and Luo X 2019 *J. Electron. Packag.* **141** 031001
[76] Ciriminna R, Fidalgo A, Pandarus V, Beland F, Ilharco L M and Pagliaro M 2013 *Chem. Rev.* **113** 6592–620
[77] Yang H *et al* 2021 *ACS Appl. Mater. Interfaces* **13** 32217–25
[78] Koushik D, Hazendonk L, Zardetto V, Vandalon V, Verheijen M A, Kessels W M M and Creatore M 2019 *ACS Appl. Mater. Interfaces* **11** 5526–35
[79] Yin B, Sadtler B, Berezin M Y and Thimsen E 2016 *Chem. Commun.* **52** 11127–30
[80] Loiudice A, Saris S, Oveisi E, Alexander D T L and Buonsanti R 2017 *Angew. Chem., Int. Ed.* **56** 10696–701
[81] Lai C F, Zhong C Z and Lee Y C 2022 *Adv. Mater. Interfaces* **9** 2201710
[82] Li Z J, Hofman E, Li J, Davis A H, Tung C H, Wu L Z and Zheng W 2017 *Adv. Funct. Mater.* **28** 1704288
[83] Xie B, Zhang J, Chen W, Hao J, Cheng Y, Hu R, Wu D, Wang K and Luo X 2017 *Nanotechnology* **28** 425204
[84] Su M, Wu D, Fan B, Wang F, Wang K and Luo Z 2018 *Dyes Pigm.* **155** 23–29
[85] Wei Y, Deng X, Xie Z, Cai X, Liang S, a M P, Hou Z, Cheng Z and Lin J 2017 *Adv. Funct. Mater.* **27** 1703535
[86] Huang H, Chen B, Wang Z, Hung T F, Susha A S, Zhong H and Rogach A L 2016 *Chem. Sci.* **7** 5699–703
[87] Xuan T, Huang J, Liu H, Lou S, Cao L, Gan W, Liu R-S and Wang J 2019 *Chem. Mater.* **31** 1042–7
[88] Raja S N, Bekenstein Y, Koc M A, Fischer S, Zhang D, Lin L, Ritchie R O, Yang P and Alivisatos A P 2016 *ACS Appl. Mater. Interfaces* **8** 35523–33
[89] Kim H Y, Yoon D-E, Jang J, Choi G-M, Lee D C and Bae B-S 2017 *J. Soc. Inf. Disp.* **25** 108–16
[90] Wang Q, Iancu N and Seo D-K 2005 *Chem. Mater.* **17** 4762–4
[91] Sun C, Shen X, Zhang Y, Wang Y, Chen X, Ji C, Shen H, Shi H, Wang Y and Yu W W 2017 *Nanotechnology* **28** 365601
[92] Jun S, Lee J and Eunjoo J 2013 *ACS Nano* **7** 1472–7
[93] Li Z, Kong L, Huang S and Li L 2017 *Angew. Chem., Int. Ed.* **56** 8134–8
[94] Shi J, Ge W, Gao W, Xu M, Zhu J and Li Y 2019 *Adv. Opt. Mater.* **8** 1901516
[95] Bockstaller M R, Mickiewicz R A and Thomas E L 2005 *Adv. Mater.* **17** 1331–49
[96] Habisreutinger S N, Leijtens T, Eperon G E, Stranks S D, Nicholas R J and Snaith H J 2014 *Nano Lett.* **14** 5561–8

[97] Leijtens T, Eperon G E, Noel N K, Habisreutinger S N, Petrozza A and Snaith H J 2015 *Adv. Energy Mater.* **5** 1500963
[98] Pei N, Yu X, Zhou S, Hu R and Luo X 2020 *IEEE Photonics Technol. Lett.* **32** 1423–6
[99] Ji H, Ye D, Xu H, Chen E and Ge Z 2022 *Opt. Mater. Express* **12** 1648–56
[100] Yu X, Pei N, Zhou S, Zhang X and Luo X 2019 *IEEE Trans. Electron Devices* **66** 5196–201
[101] Yang F, Li B, Li Y, Duan Y, Ding Y, Xiong Y and Guo S 2024 *Chem. Eng. J.* **481** 148386
[102] Xie B, Hu R and Luo X 2021 *J. Appl. Phys.* **130** 070906
[103] Zhou S, Ma Y, Zhang X, Lan W, Yu X, Xie B, Wang K and Luo X 2019 *ACS Appl. Nano Mater.* **3** 814–9
[104] Yang X, Zhou S, Xie B, Yu X, Zhang X, Xiang L, Wang K and Luo X 2021 *IEEE Electron Device Lett.* **42** 1204–7
[105] Xie B, Liu H, Hu R, Wang C, Hao J, Wang K and Luo X 2018 *Adv. Funct. Mater.* **28** 1801407
[106] Xie B, Zhao W, Luo X and Hu R 2023 *Mater. Sci. Eng.* R **154** 100738